Hydrogen Production by Alkaline Water Electrolysis Using Electrochemically Ni-Deposited Stainless Steel Electrodes

Sehnaz Genc, Serkan Karadeniz, and Nezihe Ayas*

Department of Chemical Engineering, Engineering Faculty, Eskisehir Technical University, Eskisehir, Türkiye
Email: sgenc@eskisehir.edu.tr (S.G.); skaradeniz@ogr.eskisehir.edu.tr (S.K.); nazcan@eskisehir.edu.tr (N.A.)
*Corresponding author

Manuscript received November 30, 2023; revised February 1, 2024; accepted April 3, 2024; published May 23, 2024

***Abstract*—In this study, hydrogen production capacity and energy efficiency of the alkaline water electrolysis system were improved by electrochemically modifying the Stainless-Steel (SS) electrodes. Ni metal was deposited onto the surface of SS electrodes for better cell performance. Both pristine and Ni-deposited plates were evaluated according to electrochemical cell performance, hydrogen production capacity, and energy efficiency. Additionally, X-Ray Diffraction (XRD) and Scanning Electron Microscopy (SEM) analyses were performed to investigate the crystallographic properties and surface morphology of electrodes.**

***Keywords*—water electrolysis, stainless steel, mesh, Nickel, Hydrogen**

I. Introduction

Global energy demand is increasing with each passing day, and it is essentially fueled by fossil fuels [1]. As these types of fuels are not sustainable and renewable, the development of alternatives to replace these existing fuels has been a topic of interest. Hydrogen is a clean, green, and renewable energy source with zero carbon emission, which can also be considered as a clean and renewable energy carrier with high energy density [2, 3].

Hydrogen can be produced by various methods such as gasification, natural gas reforming, and water electrolysis [4]. Water splitting by electrolysis stands out as it is a simple electrochemical process with no by-products [5]. There are several electrolysis methods namely, Alkaline Water Electrolysis (AWE), Proton Exchange Membrane electrolysis (PEM), and Solid Oxide Electrolysis (SOE). While the PEM electrolyzer requires further development to be applicable for large-scale production and SOE can be used only in kW scale, AWE is used in large-scale hydrogen production [6]. 30−40% KOH solution is widely used as electrolyte for AWE which provides electrical conductivity by decreasing the resistivity of deionized water. In AWE systems electrodes as anode and cathode are present in the alkaline electrolyte, and a membrane or diaphragm is used to separate electrodes. When a potential difference is applied to the electrodes water molecules are split into hydrogen gas and $OH^-_{(aq)}$ ions. Followed by the migration of $OH^-_{(aq)}$ ions to the anode and forming oxygen gas [7].

Alkaline water electrolysis is environmentally benign since there are no carbon emissions during the process. If the AWE system is coupled with renewable energy sources to meet the energy need, green hydrogen is produced [8]. AWE technology is a mature process with a relatively low cost compared to other electrolysis methods and is applicable for large-scale processes [9].

However, energy efficiency and sustainability of H_2 generation still face several setbacks such as the slow kinetics of Oxygen Evolution Reaction (OER) as it requires higher overpotential due to the higher reaction barrier when compared to Hydrogen Evolution Reaction (HER) [1, 3, 10, 11].

Water is split into H_2 and O_2 (Eq. 1), as HER (Eq. 2) takes place in the cathode, OER (Eq. 3) takes place in the anode [7]. The theoretical standard potential for water splitting in an electrolysis cell is 1.23 V vs. Reversible Hydrogen Electrode (RHE) and this potential is denoted as E_0.

$$H_2O \rightarrow \tfrac{1}{2}\,O_2 + H_2 \quad E_0 = 1.23\ \text{V vs. RHE} \tag{1}$$

$$2H_2O_{(l)} + 2e^- \rightarrow H_{2(g)} + 2OH^-_{(aq)} \tag{2}$$

$$2OH^-_{(aq)} \rightarrow \tfrac{1}{2}\,O_{2(g)} + 2e^- + H_2O \tag{3}$$

The thermodynamic standard potentials are not sufficient for the water electrolysis and overpotential must be applied to compensate for the energy requirement [4, 12]. In order to lower the overall cost of the water electrolysis and increase the hydrogen production per unit of consumed energy, electrode materials that are able to diminish the required overpotential must be investigated.

Pt and other noble metals such as Ru, and Ir, require low overpotentials but their extreme scarcity and high cost remain the main drawbacks regarding their use as electrocatalysts [2, 4, 11, 13–15]. Regarding these setbacks, transition group metals such as Nickel (Ni) have gained attraction as an alternative electrocatalyst. It was reported that Ni is a suitable active metal for alkaline electrolyzers as Ni is cheap and chemically stable. Rather than using pure Ni as an electrocatalyst, it can be deposited onto a substrate as a thin film to increase its activity and reduce the cost by lowering the total required metal amount. Coating Ni on a substrate was reported to be a difficult task, as the degree of adhesion varies [16].

Electrodeposition is a suitable method for Ni loading onto a substrate, where ions of a metal salt are reduced to metal state before deposition. Stainless Steel (SS) was reported as a candidate for ideal electrode material as its composition mainly consists of Fe, Cr, Mo, and Ni which make up the stainless steel and already have decent catalytic activity in electrolysis [3]. Stainless steel also has other advantages such as high electrical conductivity, corrosion/acid/temperature resistance, mechanical strength, chemical stability, and commercial availability [3, 4, 17, 18].

Stainless Steel Meshes (SSM) also offer various advantages when compared to stainless steel plates. Their high surface area, highly-ordered porosity, and ability to

allow the electrolyte and evolved gas products to pass through make them able to produce hydrogen at a faster rate than SS plates [2, 11, 15, 19, 20]. SSM is characterized by the mesh number and type, which was also reported to affect the bubble evolution and transport mechanics [14].

II. Literature Review

In the literature, there are a very limited number of studies that focus on the electrodeposition of Ni onto the SS plates and SSM for hydrogen production in alkaline water electrolysis cells [5, 10, 16, 19–21]. One recent study investigated the effect of mesh number on the HER but it was conducted in acidic media [17].

In this work, the effects of (I) type of stainless-steel electrode (Plate and two different mesh numbers), and (II) electrodeposition of Ni onto these substrates on hydrogen production by alkaline water electrolysis were investigated. Electrodes were characterized by X-Ray Diffraction (XRD), Scanning Electron Microscopy (SEM), and Energy Dispersive X-ray spectroscopy (EDX) before and after Ni electrodeposition. A homemade, two-electrode alkaline electrolysis cell was used for the activity tests. The effects of parameters during the activity tests were also evaluated and correlated to characterization results. Hydrogen production capacities of pristine SS and Ni electrodeposited SS plates at various current densities were analyzed. Polarization graphs of electrodes were compared to understand the electrochemical activity of plates.

III. Materials and Methods

Nickel nitrate hexahydrate ($Ni(NO_3)_2 \cdot 6H_2O$) (99.9%) from Zag Chemicals, Nickel (II) Chloride ($NiCl_2 \cdot 6H_2O$) (98.0%) from Merck, boric acid H_3BO_3 (99.5%) from Merck, Acetone ($(CH_3)_2CO$) (99.8%) were used directly without any modification. Ultrapure water (Milli-Q) was used in all experiments.

Stainless steel plates and meshes were AISI 304. SS plates and SSM were cut into 50 mm×35 mm rectangles. 35 mm×35 mm section providing a geometrical surface area of 1,225 mm^2 of these rectangles were used for Ni electrodeposition and hydrogen generation tests in the alkaline water electrolysis cell. The remaining area was used as a support structure and for electrical connections during electrodeposition and activity tests. 150 mesh and 250 mesh SSMs were denoted as SSM150 and SSM250, respectively.

Prior to electrodeposition, SS plates and SSMs were ultrasonicated in acetone for 10 minutes to remove any contaminants on the surface, followed by washing with ultrapure water. SS plates and SSMs were dried at 105 °C in an oven.

Electrolyte for Ni electrodeposition was prepared as described in the literature [5], using 1.143 M $Ni(NO_3)_2 \cdot 6H_2O$ and 0.323 M $NiCl_2 \cdot 6H_2O$. The electrolyte solution's pH was buffered by using 0.50 M H_3BO_3 and 0.50 M Na_2SO_4.

Electrodeposition was carried out using a DC power supply in a 250 mL cell at room temperature. Either an SS plate or SSM was used as the cathode, and the anode was an SS plate with the same active area as the cathode. Distance between electrodes was kept constant at 20 mm for all experiments. Electrodeposition duration of 20 min. and the current density of 0.8 A/dm^2 was the same for all experiments. Ni-coated SS electrodes were thoroughly washed with ultrapure water after electrodeposition and dried at 105 °C in an oven. Ni-coated SS Plate was denoted as SS Plate-Ni and the SSMs were denoted as SSM150-Ni and SSM250-Ni, respectively.

XRD was used to determine the crystallographic properties of the samples using a Rigaku XRD MiniFlex 600 using Cu Ka radiation, 2°/min scan rate, step size of 0.02° in the range of $20° < 2\theta < 100°$.

SEM imaging using a Zeiss Supra 50 VP operated at 10 kV acceleration voltage was utilized to investigate the surface morphology of SS electrodes before and after electrodeposition. EDX was also utilized to determine the composition of SS plates and SSM, before and after electrodeposition to confirm the success of Ni electrodeposition.

Electrocatalytic activity tests of electrodes were carried out to evaluate hydrogen generation performance in an alkaline water electrolysis cell. A homemade electrolysis cell consisting of two electrodes with a distance of 7 mm was used. Zirfon® membrane was used to prevent the mixing of evolved hydrogen and oxygen gases. The area of electrodes in the KOH electrolyte solution (30% wt./wt.) was 12.5 cm^2 when system sealing was provided. Two peristaltic pumps were included in the system to provide electrolyte flow. Hydrogen is collected and measured by water-gas displacement method at 0.3, 0.6, 0.9, 1.2, and 1.5 A cell current. Polarization graphs for different types of electrodes were obtained by measuring cell voltage and current between 0.0 A and 1.8 A.

The energy efficiency of the cell was evaluated according to gas production rate and consumed energy by the cell. The acquired energy worth was calculated according to the higher heating value of hydrogen and proportioned to the product of cell voltage and current to determine the percentage energy efficiency of the system.

IV. Result and Discussion

The stainless-steel plates and meshes were coated with Ni by the one-step electrodeposition method. For both SS Plates and SSMs, a constant current density of 0.8 A/dm^2 at a constant inter-electrode distance of 2 cm for 20 min. During this period, the formation of a very thin film that was darker than the electrode surface was observed. After the electrodeposition process, SS plates and SSMs were washed thoroughly with ultrapure water and dried in an oven.

SEM-EDS was utilized to investigate the microstructure of the SS Plates and SSMs. Fig. 1(a) shows the morphology and the main elements that make up the SS Plate. The surface of the SS Plate prior to electrodeposition appears cracked and relatively rough. EDS shows the existence of Fe, Cr, and Ni. Atomic ratios of Fe:Ni:Cr were 1:0.15:0.29, respectively. Fig. 1(b) shows the SS Plate after Ni electrodeposition. Ni on the surface can be described as non-homogenously distributed, aggregated nanoparticles in the form of a thin layer.

EDS analysis on the surface of SS plate where Ni electrodeposition was not observed showed that the atomic ratios of Fe:Ni:Cr were 1:0.15:0.33. Therefore, it can be concluded that the electrodeposition process does not

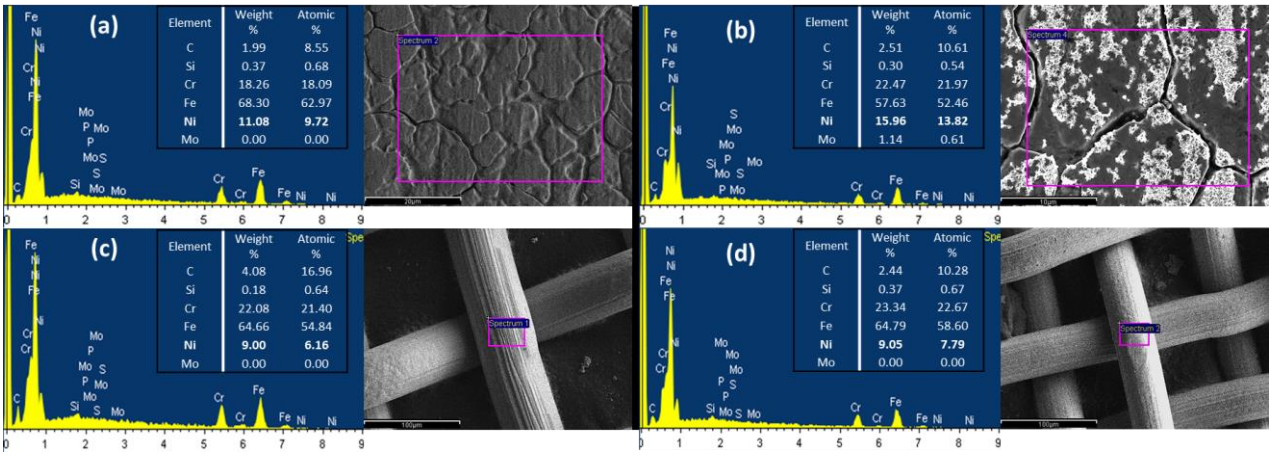

Fig. 1. EDS spectra, elemental composition, and respective SEM images of (a) Pristine SS Plate, (b) SS Plate-Ni, (c) Pristine SSM150, and (d) Pristine SSM250.

significantly alter the elemental composition of pristine SS material in the areas where no Ni electrodeposition has occurred. Investigating the areas of Ni electrodeposition, it can be seen in Fig. 1(a) and Fig. 1(b) that Ni composition by wt. increases from 11.08% to 15.96%, which corresponds to a 44% increase. Fe:Ni:Cr atomic ratios for SS Plate-Ni were 1:0.26:0.49, respectively. Higher Ni content was expected to have a higher activity in alkaline water electrolysis, which was confirmed with the electrolysis cell tests.

The pristine SS plate and Ni-coated SS plate's crystallographic structure was also investigated by XRD. Fig. 2(a) shows the XRD patterns for the Pristine SS Plate and SS Plate-Ni. Peaks near 43.6°, 50.8°, and 74.7° were attributed to 111, 200, and 220 facets of austenitic steel, respectively [3, 17, 22].

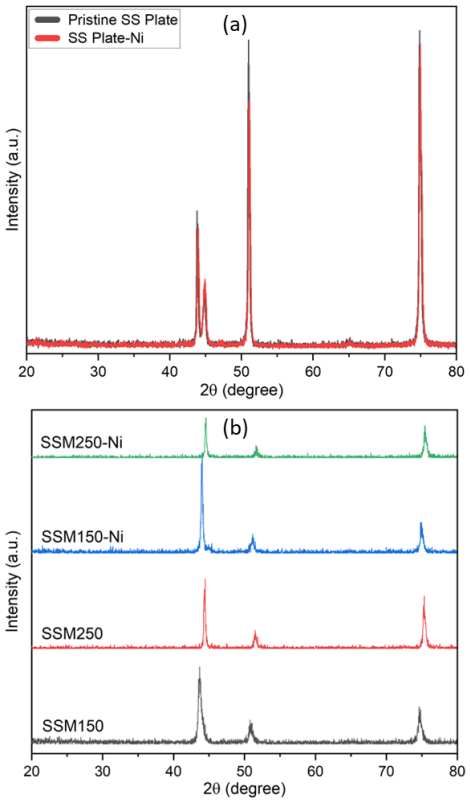

Fig. 2. XRD patterns of (a) Pristine SS Plate and Ni electrodeposited SS Plate and, (b) Pristine SSM and electrodeposited SSM.

No significant change in the overall diffraction patterns was observed after electrodeposition, indicating that the crystalline structure of the SS Plate was unchanged. A minor increase in intensity was observed for the peak near 44.8°, which indicated the successful deposition of Ni on the SS surface [11, 13].

XRD patters of SSMs are also similar to those of SS Plates, considering both materials are AISI 304 SS. The electrodeposition of Ni had no significant effect on the overall XRD pattern, considering the electrodeposited Ni was in the form of an extremely thin layer.

These results confirm the reports in the literature regarding cathodic electrodeposition of Ni from a nitrate electrolyte resulting in formation of nanocrystals with low crystallinity [20]. The reason of the minority in change of XRD pattern at 44.8° can also be explained by the low crystallinity of Ni. From Fig 1(a) and Fig 1(b) It can be seen that no significant change was observed for the surface of the SS Plate. Fe:Ni:Cr atomic ratios after electrodeposition were 1:0.26:0.42, respectively.

Fig. 1(c) and Fig. 1(d) show the elemental composition of SSM150 and SSM250, respectively. SSM150 and SSM250 have very similar elemental composition, according to EDS results. SSMs exhibit lower Fe and Ni content than SS plate but the Cr content is higher. Fe:Ni:Cr ratios for SSM150 and SSM250 are 1:0.11:0.39 and 1:0.13:0.39, respectively.

The surface morphology of SSMs was further investigated by SEM at various magnifications and the resulting images are given in Fig. 3. Only one type of wire was used for weaving the SSMs, therefore wire diameter that make up the vertical and horizontal lines was the same for the specific SSM.

SSMs have a higher surface area than the SS Plate due to their porous structure, therefore surface areas of SSMs were calculated by using a method found in the literature [14]. Wire diameter (d) and average distance between the wires (L) were measured from SEM images to calculate the surface areas of SSMs. SSM150 (d = 62 μm, L = 111 μm) and SSM250 (d = 46 μm, L = 56 μm) have a surface area factor of 13.95 cm^2/cm^2 and 16.72 cm^2/cm^2, respectively. A comparison of the surface areas for SS Plate and SSM electrodes with a total geometrical area of 12.25 cm^2 (3.5 cm×3.5 cm) is given in Table 1. The area for the SS Plate was doubled, considering the electrodeposition was conducted for both sides of the electrode.

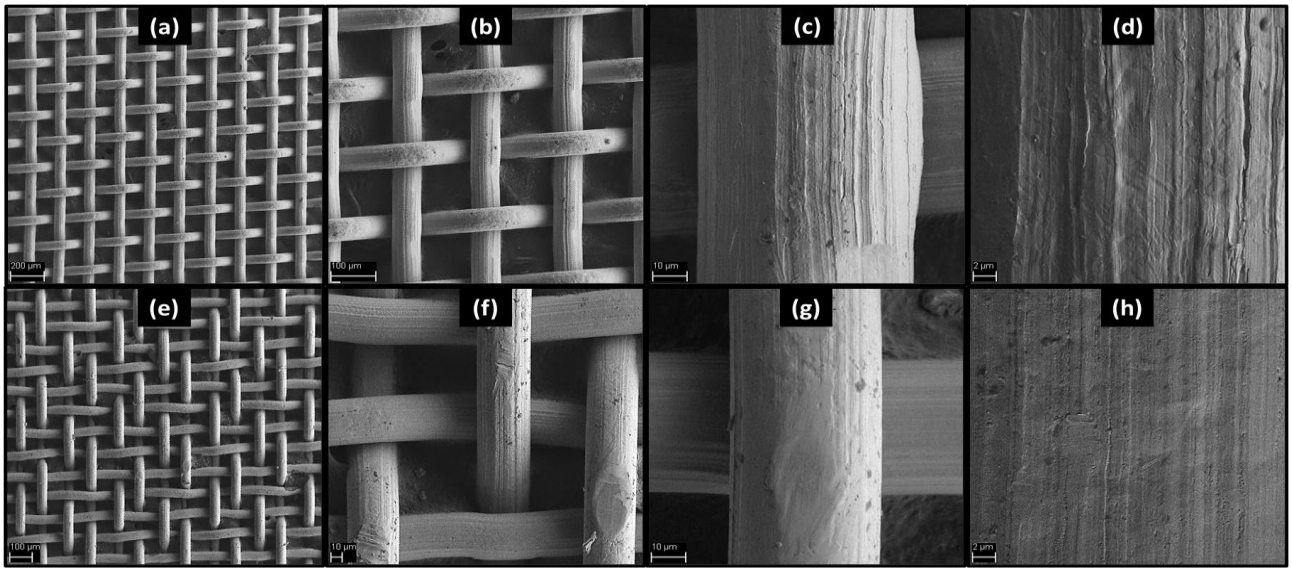

Fig. 3. SEM images at various magnifications for Pristine (a)–(d) SSM150 and, (e)–(h) SSM250.

Table 1. Total surface areas for SS plate and SSM electrodes for electrodeposition

	Electrode Type		
	SS Plate	**SSM150**	**SSM250**
Area Factor (cm^2/cm^2)	1	13.95	16.72
Total Area (cm^2)	24.5	170.89	204.82

Electrodes were tested in alkaline water electrolysis cell to obtain electrochemical behavior and hydrogen production rates of different types of electrodes. In Fig. 4(a), polarization curves for pristine SS and Ni-deposited SS plates were shown. According to the results, SS Plate-Ni performed better electrochemical activity in the cell. Current density values are higher than pristine SS at the same cell voltage. Depositing Ni onto SS plates increased the cell performance between 0.0–0.144 A/cm^2 of current densities.

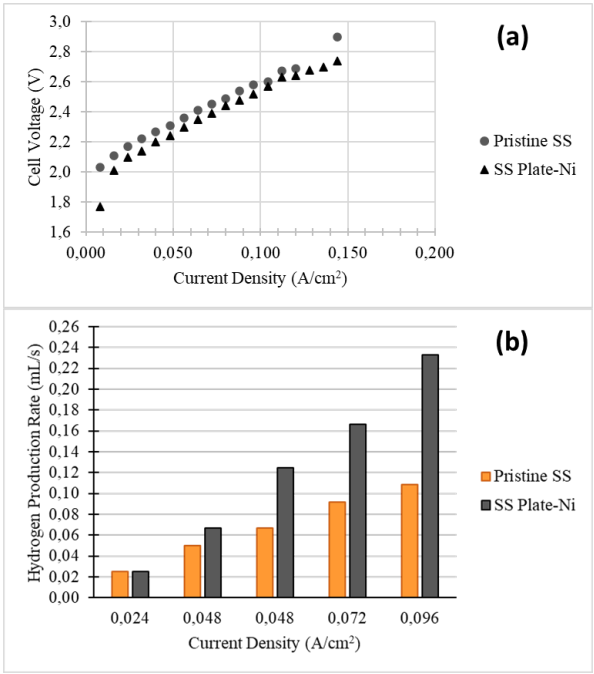

Fig. 4. (a) Polarization graph of an electrolysis cell for Pristine SS Plate and SS Plate-Ni, (b) Hydrogen production rates of Pristine SS and SS Plate-Ni.

As seen from Fig. 4(b) hydrogen production rate of the cell raised as the cell current was increased. It was concluded that Ni-deposited plates have greater hydrogen production capacity than pristine ones. The hydrogen production rate difference between pristine and deposited plates becomes more significant with the increased current density.

SEM images of SSM150-Ni and SSM250-Ni are given in Fig. 5. Both SSMs show a more uniform Ni coating than the SS Plate-Ni. The order of uniformity is SSM250-Ni > SSM150-Ni > SS Plate-Ni. Low magnification images in Fig. 5(a), (b), (g), and (h) show that all the surfaces of SSMs were successfully coated with Ni.

Comparing the high magnification images in Fig. 5 (c), (d), (i), and (j), SSM150-Ni show a higher degree of Ni agglomeration and these agglomerations are formed parallel to the wire orientation. These agglomerations are thinner for SSM250-Ni and the small and segregated deposits of Ni make up for more of the surface coating. Near circular deposits observed in Fig. 5(d) have an average diameter of 118±14 nm, while the circular deposits in Fig. 5(j) are in the range of 126±16 nm. The size of the smallest units of Ni deposits are nearly the same for both meshes, but SSM250-Ni has a much more uniform distribution, resulting in fewer agglomerations. EDS results given in Fig. 5(e) and Fig. 5(f) also confirm the observed depositions are Ni. Uniform deposition of Ni in SSM250-Ni changes the Fe:Ni:Cr ratio from 1:0.13:0.39 to 1:0.36:0.54.

In Fig. 6, the energy efficiency of the electrolysis cell can be observed. While energy efficiencies were between values of 30–40% for pristine electrodes, Ni deposited electrodes performed 46–68% efficiency. Ni deposition enabled hydrogen production by consuming less energy compared to pristine electrodes.

The results in Fig. 6 also indicated that energy efficiency of the system had a tendency of decreasing for pristine electrodes as the current density increased. However, vice versa trend was obtained when Ni deposited electrodes were used. The energy efficiency of the system reached nearly the maximum of 70% along with increasing current density.

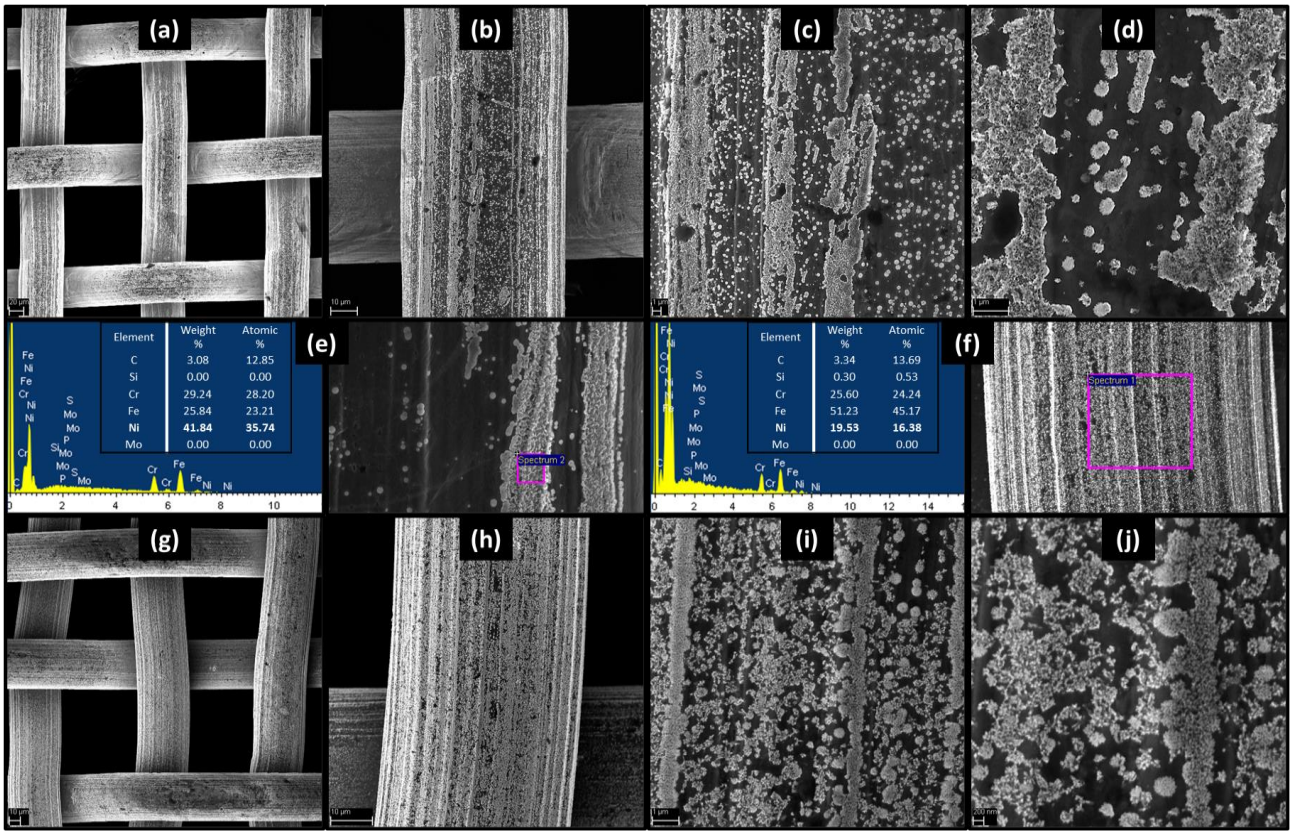

Fig. 5. SEM images at different magnifications for; (a)–(d) SSM150-Ni and, (g)–(j) SSM250-Ni. EDS spectra, elemental composition, and respective SEM image for (e) SSM150-Ni and, (f) SSM250-Ni.

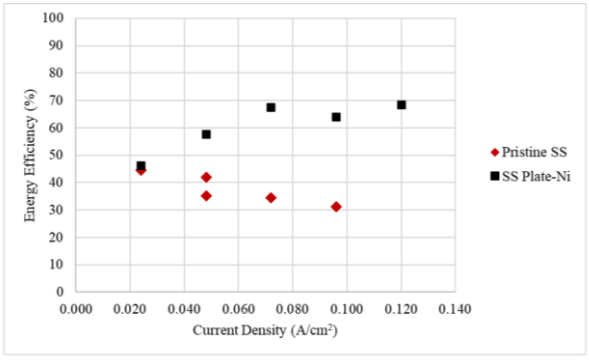

Fig. 6. Energy efficiency of the alkaline water electrolysis cell.

Economic advantage of Ni deposited SS plates was considerable. Compared to Nickel, Irons is more abundant and 50 times cheaper [23]. Therefore, using steel as electrode material is a cost-effective material for hydrogen production. Decreasing the capital expenses for alkaline water electrolysis prevails the way of competitiveness with fossil fuel-based technologies. However, the activity of stainless steel should also be increased for larger hydrogen production capacity. In this study, steel electrode surfaces were coated by consuming Nickel salts and resulted in 80% increase of hydrogen production rate at 0.096 A/cm^2 current density. Therefore, instead of using pure Nickel or pure steel, deposited plates with less cost and higher activity achieve a boost in fuel (hydrogen) production.

The performance of the SSMs could not be evaluated using the current electrolysis system, as the generated hydrogen and oxygen produce a cushioning effect, therefore breaking the electrical connection between the electrodes. The design of a system that can overcome this effect is planned and is subject for future work.

V. Conclusion

This work was conducted to evaluate the performance effects of Ni electrodeposition on the stainless-steel plates and meshes for the alkaline water electrolysis. Results show that Ni electrodeposition becomes more uniform as the mesh number increases. SSM250-Ni has the most uniform distribution of Ni deposits while SS Plate-Ni shows a much more pronounced Ni agglomeration. Electrochemical performance of the cell was enhanced by using Ni deposited electrodes compared to pristine ones. Additionally, Ni electrodeposition on SS Plate nearly doubles the rate of hydrogen production and increase in energy efficiency was observed for alkaline water electrolysis. It can be concluded that SSMs provide a promising alternative to plate-type SS electrodes and their performance can be further improved by active metal electrodeposition.

Conflict of Interest

The authors declare no conflict of interest.

Author Contributions

S. Genc and S. Karadeniz conducted the lab work and devised the methodology for experiments and analysis. Preparation of the original and revised manuscript was done by S. Karadeniz. Throughout the research progress, N. Ayas provided their supervision and guidance. All authors had approved the final version.

FUNDING

This work was supported by the Eskisehir Technical University (ESTU) Scientific Research Projects Commission, grant number 22ADP318.

ACKNOWLEDGMENT

The authors would like to thank the ESTU Materials Science and Engineering Department for their equipment support for SEM and XRD analysis.

REFERENCES

[1] X. Lyu *et al.*, "Investigation of oxygen evolution reaction with Ni foam and stainless-steel mesh electrodes in alkaline seawater electrolysis," *Journal of Environmental Chemical Engineering*, vol. 10, no. 5, 108486, Oct. 2022. doi: 10.1016/j.jece.2022.108486

[2] B. Ghasemi, S. Yaghmaei, K. Abdi, M. M. Mardanpour, and S. A. Haddadi, "Introducing an affordable catalyst for biohydrogen production in microbial electrolysis cells," *Journal of Bioscience and Bioengineering*, vol. 129, no. 1, pp. 67–76, Jan. 2020. doi: 10.1016/j.jbiosc.2019.07.001

[3] B. Liu, C. Shen, L. Min, L. Liu, W. Zhang, and Y. Wang, "Electroplated Ni-Fe layer on stainless steel fiber felt as an efficient electrode for oxygen evolution reaction," *International Journal of Electrochemical Science*, vol. 17, no. 6, 220652, Jun. 2022. doi: 10.20964/2022.06.47

[4] A. F. Alharbi, A. A. M. Abahussain, W. Wazeer, H. El-Deeb, and A. B. A. A. Nassr, "Stainless steel as gas evolving electrodes in water electrolysis: Enhancing the activity for hydrogen evolution reaction via electrodeposition of Co and CoP catalysts," *International Journal of Hydrogen Energy*, vol. 48, no. 80, pp. 31172–31186, Sep. 2023. doi: 10.1016/j.ijhydene.2023.04.228

[5] M. I. Jaramillo-Gutiérrez, S. M. Sierra-González, C. A. Ramírez-González, J. E. Pedraza-Rosas, and J. A. Pedraza-Avella, "Effect of electrodeposition parameters and surface pretreatment on the electrochemical hydrogen production using Nickel-plated stainless steel electrodes," *International Journal of Hydrogen Energy*, vol. 46, no. 11, pp. 7667–7675, Feb. 2021. doi: 10.1016/j.ijhydene.2019.09.205

[6] M. El-Shafie, "Hydrogen production by water electrolysis technologies: A review," *Results in Engineering*, vol. 20, 101426, Dec. 2023. doi: 10.1016/j.rineng.2023.101426

[7] M. David, C. Ocampo-Martínez, and R. Sánchez-Peña, "Advances in alkaline water electrolyzers: A review," *Journal of Energy Storage*, vol. 23, pp. 392–403, Jun. 2019. doi: 10.1016/j.est.2019.03.001

[8] J. Brauns and T. Turek, "Alkaline water electrolysis powered by renewable energy: A Review," *Processes*, vol. 8, no. 2, p. 248, Feb. 2020. doi: 10.3390/pr8020248

[9] Y. Guo, G. Li, J. Zhou, and Y. Liu, "Comparison between hydrogen production by alkaline water electrolysis and hydrogen production by PEM electrolysis," *IOP Conf. Ser.: Earth Environ. Sci.*, vol. 371, no. 4, 042022, Dec. 2019. doi: 10.1088/1755-1315/371/4/042022

[10] J. Shen, M. Wang, L. Zhao, P. Zhang, J. Jiang, and J. Liu, "Amorphous Ni(Fe)OH-coated nanocone arrays self-supported on stainless steel mesh as a promising oxygen-evolving anode for large scale water splitting," *Journal of Power Sources*, vol. 389, pp. 160–168, Jun. 2018. doi: 10.1016/j.jpowsour.2018.04.023

[11] L. Li, J. Long, Q. Ye, X. Xu, and F. Wang, "Ni-Co layered double-hydroxide arrays on stainless steel substrate: Interfacial hydroxide layer enhanced electrocatalyst with high stability for oxygen evolution reaction in alkaline media," *Journal of Alloys and Compounds*, vol. 946, 169325, Jun. 2023. doi: 10.1016/j.jallcom.2023.169325

[12] X. Lyu, Y. Bai, J. Li, R. Tao, J. Yang, and A. Serov, "Investigation of oxygen evolution reaction with 316 and 304 stainless-steel mesh electrodes in natural seawater electrolysis," *Journal of Environmental Chemical Engineering*, vol. 11, no. 3, 109667, Jun. 2023. doi: 10.1016/j.jece.2023.109667

[13] A. A. Kashale *et al.*, "Thermally constructed stable Zn-doped NiCoOx-z alloy structures on stainless steel mesh for efficient hydrogen production via overall hydrazine splitting in alkaline electrolyte," *Journal of Colloid and Interface Science*, vol. 640, pp. 737–749, Jun. 2023. doi: 10.1016/j.jcis.2023.02.142

[14] Y. Zhang, M. D. Merrill, and B. E. Logan, "The use and optimization of stainless steel mesh cathodes in microbial electrolysis cells," *International Journal of Hydrogen Energy*, vol. 35, no. 21, pp. 12020–12028, Nov. 2010. doi: 10.1016/j.ijhydene.2010.08.064

[15] W. H. Yun, Y. S. Yoon, H. H. Yoon, P. K. T. Nguyen, and J. Hur, "Hydrogen production from macroalgae by simultaneous dark fermentation and microbial electrolysis cell with surface-modified stainless steel mesh cathode," *International Journal of Hydrogen Energy*, vol. 46, no. 79, pp. 39136–39145, Nov. 2021. doi: 10.1016/j.ijhydene.2021.09.168

[16] F. J. Pérez-Alonso, C. Adán, S. Rojas, M. A. Peña, and J. L. G. Fierro, "Ni/Fe electrodes prepared by electrodeposition method over different substrates for oxygen evolution reaction in alkaline medium," *International Journal of Hydrogen Energy*, vol. 39, no. 10, pp. 5204–5212, Mar. 2014. doi: 10.1016/j.ijhydene.2013.12.186

[17] Y. Liu *et al.*, "Industrial stainless steel meshes for efficient electrocatalytic hydrogen evolution," *Journal of Energy Storage*, vol. 41, 102844, Sep. 2021. doi: 10.1016/j.est.2021.102844

[18] M. Su, L. Wei, Z. Qiu, G. Wang, and J. Shen, "Hydrogen production in single chamber microbial electrolysis cells with stainless steel fiber felt cathodes," *Journal of Power Sources*, vol. 301, pp. 29–34, Jan. 2016. doi: 10.1016/j.jpowsour.2015.09.108

[19] G. A. Gebreslase, M. V. Martínez-Huerta, D. Sebastián, and M. J. Lázaro, "NiCoP/CoP sponge-like structure grown on stainless steel mesh as a high-performance electrocatalyst for hydrogen evolution reaction," *Electrochimica Acta*, vol. 438, 141538, Jan. 2023. doi: 10.1016/j.electacta.2022.141538

[20] S.-B. Yang, Y.-C. Tsai, and M.-S. Wu, "Honeycomb-like copper/cuprous oxide with supported nickel hydroxide layer as an electrode material for electrochemical oxidation of urea," *Journal of Alloys and Compounds*, vol. 836, 155533, Sep. 2020. doi: 10.1016/j.jallcom.2020.155533

[21] F. A. Soriano Moranchell, J. M. Sandoval Pineda, J. N. Hernández Pérez, U. S. Silva-Rivera, C. A. Cortes Escobedo, and R. D. G. González Huerta, "Electrodes modified with Ni electrodeposition decrease hexavalent chromium generation in an alkaline electrolysis process," *International Journal of Hydrogen Energy*, vol. 45, no. 26, pp. 13683–13692, 2020. doi: 10.1016/j.ijhydene.2020.01.050

[22] N. Karthik, R. Atchudan, T. N. J. I. Edison, and S. T. Choi, "Insights of pristine stainless steel mesh oxygen evolution reaction in diverse concentrations of potassium hydroxide," *Materials Letters*, vol. 333, 133557, Feb. 2023. doi: 10.1016/j.matlet.2022.133557

[23] B. Zayat, D. Mitra, and S. R. Narayanan, "Inexpensive and efficient alkaline water electrolyzer with robust steel-based electrodes," *J. Electrochem. Soc.*, vol. 167, no. 11, 114513, Jan. 2020. doi: 10.1149/1945-7111/aba792